DEVELOPMENT OF ADVANCED CFD

A Generalized Framework for Adjoint Error Estimation of PG Method Applied to Linear Problems

Stefano D'Angelo

Aeronautics and Aerospace Department, von Karman Institute for Fluid Dynamics, Belgium, dangelo@vki.ac.be

Supervisor: Herman Deconinck

Professor, Aeronautics and Aerospace Department, von Karman Institute for Fluid Dynamics, Belgium, deconinck@vki.ac.be

University Supervisor: Mario Ricchiuto

Research Engineer, INRIA Bordeaux - Sud-Ouest, France, mario.ricchiuto@inria.fr

Abstract

The current work concerns the study and the implementation of a modern algorithm for error estimation in Computational Fluid Dynamics (CFD) computations. This estimate involves the use of the adjoint argument. By solving the adjoint problem, it is possible to gain important information about the transport of the error related to the quantity of interest. The aim is to apply for the first time this procedure to the Petrov-Galerkin (PG) method. Some numerical schemes such as Streamline Upwind Petrov-Galerkin (SUPG), stabilized Residual Distribution (RD) and bubble method have been selected for implementation and tested. Scalar linear hyperbolic problems are used as basic demostration.

Keywords: error estimation, adjoint problem, hyperbolic problem, Petrov-Galerkin

1. Introduction

Over the last decade, much progress has been made in the area of error estimation. This theory provides a way to construct error indicators for CFD computations of PDE's. These indicators can be used to drive automatic mesh adaptation algorithms, by optimizing the mesh spacings or reducing the memory usage.
In this field, the *a posteriori* error analysis is one of the most used procedures to compute numerical error indicators. The relevance and generality of this estimation has been powerfully argued in the work of Johnson and his collaborators [1]. The *a posteriori* error bounds resulting from this analysis involve the numerical residual, obtained by inserting the computed solution into the current problem equations; this residual measures the extent to which the numerical approximation to the continuous solution fails to satisfy the current problem. From this study, the *Type II a posteriori* error bounds have been defined.
Becker and Rannacher worked also on this issue, developing the so-called weighted-residual-based, or *Type I*, *a posteriori* error estimation ([2] and [3]). Here, the error representation formula defines the error in the target functional for the numerical residual, weighted by the solution of an adjoint problem. The key ingredient is this auxiliary problem, involving the formal adjoint of the current partial differential operator. For computing this product, also the adjoint problem will be implemented and solved numerically. To solve this problem, added cost rises. However, it is paid back by important information which helps to identify the real source of the error. For example, Hartmann ([4]) shows the relevance and the advantages of *Type I* indicators over the *Type II* for the adaptive mesh design for a supersonic flow past an airfoil.
The data for the adjoint problem is a quantity of interest depending on the application. In engineering applications, this is typically a functional of the analytical solution such as a mean, point value or boundary flux. In fluid dynamics, it may be the pressure at the stagnation point, the pressure-drop between inflow and outflow or the drag or lift coefficients of a body immersed into the fluid.

2. Definition in continuous setting

2.1. Primal and adjoint problem

Primal problem model. Let Ω be a bounded open domain R^d with boundary Γ. Given the *primal problem* in strong form

$$Lu = f \quad \text{in} \quad \Omega \qquad Bu = g \quad \text{on} \quad \Gamma \tag{1}$$

where $f \in L^2(\Omega)$ and $g \in L^2(\Gamma)$, L denotes a linear differential operator on Ω and B a linear boundary operator on Γ.

The functional $J(\cdot)$. In many problems of physical interest the quantity of interest for the current problem is an output or target functional of the solution rather the solution itself. This target functional is defined as $J(\cdot)$. Depending on the problem, it can be a different quantity, for example the drag or the lift coefficient or a point value of the solution.
According to the theory, the linear functional is defined by

$$J(u) = (u, j_\Omega)_\Omega + (Cu, j_\Gamma)_\Gamma \tag{2}$$

where $j_\Omega \in L^2(\Omega)$ and $j_\Gamma \in L^2(\Gamma)$ and C is a differential boundary operator on Γ and $(\cdot,\cdot)_\Omega$ and $(\cdot,\cdot)_\Gamma$ denote the $L^2(\Omega)$ and $L^2(\Gamma)$ inner products respectively.

Associated adjoint problem. Following the theory of adjoint operators [5] we can write the (continuous) *compatibility equation*, for $\forall v \in H^1$

$$(Lu, v)_\Omega + (Bu, C^* v)_\Gamma = (u, L^* v)_\Omega + (Cu, B^* v)_\Gamma \tag{3}$$

where, L, B and C are the operators of the primal problem and L^*, B^* and C^* the corresponding adjoint counterparts. By these so-called *adjoint operators*, we build the adjoint problem associated to (1)

$$L^* z = j_\Omega \quad \text{in} \quad \Omega, \qquad B^* z = j_\Gamma \quad \text{on} \quad \Gamma. \tag{4}$$

Terms j_Ω and j_Γ on the right-hand side depend on the target quantity that we want to investigate. From the (3), we note that for given operators L and B associated with the primal problem (1) only some target functionals (2) with operator C are compatible whereas others are not. Moreover, in an adjoint-based optimization framework, [6], there ensures that

$$\begin{aligned} J(u) &= (u, j_\Omega)_\Omega + (Cu, j_\Gamma)_\Gamma = (u, L^* v)_\Omega + (Cu, B^* v)_\Gamma \\ &= (Lu, v)_\Omega + (Bu, C^* v)_\Gamma = (f, z)_\Omega + (g, C^* z)_\Gamma \end{aligned}$$

The associated adjoint problem describes how the information is transported towards the current quantity of interest. This is extremely useful to derive where and how the source of the error of the target quantity is carried over the domain. The error indicator derived by this information will allow to trace sources of the error of the quantity of interest.

3. Numerical discretization

Let Ω be subdivided into a shape-regular mesh $\mathcal{K} = \{\kappa\}$ consisting of elements κ. Let $\mathcal{V}_{h,p}$ be the standard finite element space of piecewise polynomials of complete degree p with C^0 continuity between elements

$$\mathcal{V}_{h,p} = \{v_h : v_h \in C^0(\Omega), v_h|_\kappa \in \mathcal{P}_p(\kappa), \forall \kappa \in \mathcal{K}\} \tag{5}$$

with $\mathcal{P}(\kappa)$ the space of polynomials of degree $\leq p$ defined on an element κ. Let then define a second space $\mathcal{V}^b_{h,q}$ which is the mesh dependent broken space of piecewise polynomials of complete degree q in each κ with no continuity between elements

$$\mathcal{V}^b_{h,q} = \{v_b : v_b|_\kappa \in \mathcal{P}_q(\kappa), \forall \kappa \in \mathcal{K}\} \tag{6}$$

We discretize both primal and adjoint problem and solve them numerically by using a *Petrov-Galerkin* (PG) method, where trial and test functions belong to $\mathcal{V}_{h,p}$ and $\mathcal{V}^b_{h,q}$, respectively, depending on the current problem.
According to (5) and (6), the boundary conditions are not imposed by the functional spaces, hence they have ti be added explcitly to the weak formulation of the problem.
Then following (3), the (discrete) compatibility condition holds as follows, for $\forall v_b \in \mathcal{V}^b_{h,p}$

$$\begin{aligned} (Lu_h, v_b)_\Omega + (Bu_h, C^* v_b)_\Gamma \quad = \\ (u_h, L^* v_b)_\Omega + (Cu_h, B^* v_b)_\Gamma + \sum_k (H(u_h, \boldsymbol{n}), v_b^+)_{\partial\kappa\setminus\Gamma} \end{aligned} \tag{7}$$

The additional terms in the RHS represents the effect of the broken test space when applying partial integration to the LHS, leading to jump terms over the element boundaries. Thus, for a conservation law, $H(w_h, \boldsymbol{n})$ is the numerical flux over $\partial\kappa$, which is unconditionally continuous because the $w_h \in \mathcal{V}_{h,p}$, $\boldsymbol{n}$ is the outward normal along the element boundary and v_b^+ the outward traces of v_b over $\partial\kappa$.
So we can define a bilinear operator $\mathcal{B}(\cdot,\cdot)$ as

$$\mathcal{B}(u_h, v_b) = (Lu_h, v_b)_\Omega + (Bu_h, C^* v_b)_\Gamma \tag{8}$$

Then, defining $F(\cdot)$ a linear form including the prescribed primal force and boundary data functions, f and g, the (discrete) primal problem is defined as

PRIMAL PROBLEM Find $u_h \in \mathcal{V}_{h,p}$ such that

$$\mathcal{B}(u_h, v_b) = F(v_b) \qquad \forall v \in \mathcal{V}^b_{h,q} \tag{9}$$

while the corresponding adjoint problem is given by

ADJOINT PROBLEM Find $z_b \in \mathcal{V}^b_{h,q}$ such that

$$\mathcal{B}(w_h, z_b) = J(w_h) \qquad \forall w_h \in \mathcal{V}_{h,p} \tag{10}$$

As we see, both problems use the same operator $\mathcal{B}(\cdot,\cdot)$, as in Discontinuous Galerkin (DG) methods. However due to the Galerkin properties, in the DG discretization test and trial space are identical, instead here, in the primal problem the solution $u_h \in \mathcal{V}_{h,p}$ and the test function v_b belongs to $\mathcal{V}^b_{h,p}$ while for the adjoint problem, the solution $z_b \in \mathcal{V}^b_{h,q}$ and the test function w_h is taken from $\mathcal{V}_{h,q}$.

3.1. Broken space $\mathcal{V}^b_{h,q}$

A plethora of possible Broken spaces $\mathcal{V}^b_{h,q}$ are available. Herebelow we list the three Petrov-Galerkin spaces that will be taken into account for the computations considered in section (5). Therefore, let remind that for a PG method, the broken spaces $\mathcal{V}^b_{h,q}$ can be always defined by a sum of two contributions

$$\mathcal{V}^b_{h,q} = \text{span}\{\Psi^0 + \Psi^1\}$$

where Ψ^0 is the "main" shape function of the space and Ψ^1 is a element stabilizer term.

Streamline Upwind Petrov-Galerkin method. In case of a Streamline Upwind Petrov-Galerkin (SUPG) method, the broken space $\mathcal{V}^b_{h,q}$ is the same as $\mathcal{V}_{h,p}$ except for the addition of a stabilizer term

$$\mathcal{V}^b_{h,q} = \text{span}\{\varphi^q_i + \tau_\kappa \boldsymbol{b} \cdot \nabla\varphi^q_i\} \tag{11}$$

where τ_κ is usually the size of the element κ and $\varphi^q_i \in \mathcal{V}_{h,q}$ the Lagrange interpolant polynomial of the degree of freedom, i, and order q; while, finally, $\boldsymbol{b}$ is the local advection speed of the current problem. So for this functional space $\Psi^0_j = \varphi^q_j$ and $\Psi^1_j = \tau_\kappa \boldsymbol{b} \cdot \nabla\varphi^q_j$.

Residual-Distribution Method. If the stabilised Residual Distribution (RD) space is chosen, the broken space, $\mathcal{V}^b_{h,q}$, is defined as

$$\mathcal{V}^b_{h,q} = \text{span}\{\beta_i + \tau_\kappa \boldsymbol{b} \cdot \nabla\varphi^q_i\} \quad \text{for} \quad q > 1 \tag{12}$$

where $\beta_i(x) = \beta^\kappa_i(\{k_i\}_{i\in\kappa}, u_h, \boldsymbol{b}, h, Lu_h|_\kappa)$ and $k_i = L\varphi_i$; while τ_κ is usually the size of the element κ and φ^q_i the Lagrange interpolant polynomial of the degree of freedom, i, and order q. So $\Psi^0_j = \chi^\kappa\beta^\kappa_j$ and $\Psi^1_j = \tau_\kappa \boldsymbol{b} \cdot \nabla\varphi^q_j$.

"Bubble" method. The "bubble" method comes out from the equivalence of the RD and SUPG method. Indeed, it takes the following broken space $\mathcal{V}^b_{h,q}$

$$\mathcal{V}^b_{h,q} = \text{span}\{\varphi^q_i + S^\kappa\alpha^\kappa_i\} \tag{13}$$

with φ^q_i the Lagrange interpolant polynomial of the degree of freedom, i, and order q, while S^κ is a bubble function vanishing along $\partial\kappa$. In this case, it is either a linear bubble, unary in the baricentric point $\boldsymbol{x}_g$, or a cubic one, coming out from the product of the three vertex linear functions. Finally α^κ_i is given by $\alpha^\kappa_i = \beta_i - \phi_i$, where β_i is the corresponding RD basis function. Then here $\Psi^0_j = \varphi^q_j$ and $\Psi^1_j = S^\kappa\alpha^\kappa_i$.

3.2. Numerical analysis

Consistency and adjoint consistency. All Petrov-Galerkin methods satisfy the *Galerkin orthogonality*

$$\mathcal{B}(u - u_h, v_b) = 0 \tag{14}$$

for $\forall v \in \mathcal{V}^b_{h,p}$ which means that the discretization error $e = u - u_h$ is orthogonal (with respect to the bilinear form $\mathcal{B}$) to the discrete test space $\mathcal{V}^b_{h,p}$. Hence, because $v \in \mathcal{V}^b_{h,p} \subset \mathcal{V}$, we find for $\forall v \in \mathcal{V}$

$$\mathcal{B}(u, v) = F(v) \tag{15}$$

This proves that a PG method is a *consistent* discretization of the primal problem (1). Furthermore, a numerical discretization is called also *adjoint consistent* [5], if the exact solution $z \in \mathcal{V}$ to the adjoint problem (4) satisfies, for $\forall w \in \mathcal{V}$

$$\mathcal{B}(w, z) = J(w) \tag{16}$$

In other words, the discrete adjoint problem is a consistent discretization of the continuous adjoint problem. Motivated by the identity (7) and replacing z_b by the exact solution z and because $w_h \in \mathcal{V}_{h,p} \subset \mathcal{V}$, we can state that the bilinear form $\mathcal{B}$ is also adjoint consistent.

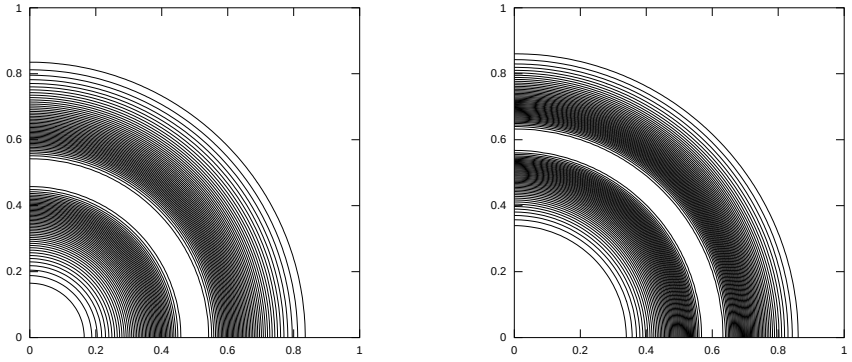

(a) (b)

Figure 1: Barth's problem : (a) primal; (b) adjoint

Method	h	$\|u-u_h\|_{L^2}$		$\|z-z_h\|_{L^2}$		$\|J(u)-J(u_h)\|$	
SUPG	.0312	3.8562e-03		5.3264e-03		5.8600e-05	
SUPG	.0156	8.9181e-04	(2.11)	1.8667e-03	(1.51)	8.9990e-06	(2.70)
SUPG	.0078	1.5552e-04	(2.52)	3.6204e-04	(2.37)	1.1747e-06	(2.94)
SUPG	.0039	2.5720e-05	(2.60)	6.2955e-05	(2.52)	1.4700e-07	(3.00)
RD-LDA	.0312	3.9011e-03		1.0118e-02		2.2153e-04	
RD-LDA	.0156	1.1269e-03	(1.79)	3.3506e-03	(1.59)	5.7671e-05	(1.94)
RD-LDA	.0078	2.9220e-04	(1.95)	9.7188e-04	(1.79)	1.5135e-05	(1.93)
RD-LDA	.0039	7.4076e-05	(1.98)	2.8564e-04	(1.77)	3.8672e-06	(1.97)
BUBBLE	.0312	2.6321e-03		5.0281e-03		9.6111e-05	
BUBBLE	.0156	6.0996e-04	(2.11)	1.5697e-03	(1.68)	2.5721e-05	(1.90)
BUBBLE	.0078	1.4730e-04	(2.05)	3.9956e-04	(1.97)	6.7168e-06	(1.94)
BUBBLE	.0039	3.5841e-05	(2.04)	1.1083e-04	(1.85)	1.7109e-06	(1.97)

Table 1: Convergence rates $p = 1$ order of SUPG, RD and BUBBLE methods for cicular advection problem [7].

Method	h	$\|u-u_h\|_{L^2}$		$\|z-z_h\|_{L^2}$		$\|J(u)-J(u_h)\|$	
SUPG	.0312	2.6300e-04		7.2814e-04		5.6795e-07	
SUPG	.0156	3.2645e-05	(3.01)	9.9617e-05	(2.87)	2.2024e-08	(4.69)
SUPG	.0078	2.8945e-06	(3.50)	1.0450e-05	(3.25)	7.4814e-10	(4.88)
SUPG	.0039	3.1390e-07	(3.20)	1.0542e-06	(3.31)	2.3627e-11	(4.98)
RD-LDA	.0312	3.7591e-04		5.8481e-03		2.1472e-06	
RD-LDA	.0156	8.1254e-05	(2.21)	3.1556e-03	(0.89)	2.7553e-07	(2.96)
RD-LDA	.0078	1.5478e-05	(2.39)	1.7036e-03	(0.89)	3.7701e-08	(2.87)
RD-LDA	.0039	2.5365e-06	(2.61)	9.1564e-04	(0.90)	4.7701e-09	(2.98)
BUBBLE	.0312	1.7989e-04		6.7172e-03		4.2105e-06	
BUBBLE	.0156	3.7848e-05	(2.25)	4.3264e-03	(0.63)	6.5782e-07	(2.68)
BUBBLE	.0078	8.3242e-06	(2.18)	2.5741e-03	(0.75)	8.9382e-08	(2.88)
BUBBLE	.0039	1.6420e-06	(2.34)	1.4398e-03	(0.84)	1.1594e-08	(2.95)

Table 2: Convergence rates $p = 2$ order of SUPG, RD and BUBBLE methods for cicular advection problem [7].

Convergence (order of convergence). Let $u \in H^{p+1}(\Omega)$ and $u_h \in \mathcal{V}_{h,p}$ be the solutions to (15) and (1), respectively. Then,

$$\|u - u_h\|_{L^2(\Omega)} \leq Ch^{p+1}|u|_{H^{p+1}(\Omega)} \tag{17}$$

Let $p \geq 0$ and $\mathcal{V}^b_{h,p}$ be the broken finite element space defined in (6). Then, by $P^b_{h,p}$ we denote the L^2-projection onto $\mathcal{V}^b_{h,p}$, i.e. given a $u \in L^2(\Omega)$ we define $P^b_{h,p}u \in \mathcal{V}^b_{h,p}$ by

$$\int_\Omega (u - P^b_{h,p}u)v_h \, d\boldsymbol{x} = 0 \quad \forall v_h \in \mathcal{V}^b_{h,p}$$

we use the short notation $P_h u$ instead of $P^b_{h,p}u$ when it is clear which projection is meant. Now, let $p \geq 0$ and $P_h v$ be the L^2-projection. Suppose $v \in H^{p+1}(\Omega)$, then

$$\|v - P_h v\|_{H^{p+1}(\Omega)} \leq Ch\|v\|_{L^2(\Omega)} \tag{18}$$

To numerically verify the convergence rate for smooth primal and adjoint data, numerical solutions of the following 2-D circular advection problem [7] were obtained

$$\begin{aligned} \boldsymbol{b} \cdot \nabla u &= 0 \quad \text{in } \Omega \\ u &= g \quad \text{on } \Gamma_- \end{aligned} \tag{19}$$

The target quantity is the weighted outflow flux functional

$$J(u) = \int_0^1 \delta_+(\boldsymbol{b} \cdot \boldsymbol{n})\psi_{\text{outflow}} u \, d\boldsymbol{x}$$

Figures 1a and 1b show primal and adjoint current solutions, respectively, while tables 1 and 2 tabulate values of the global solution error using a sequence of four nested meshes. Here, the $p + 1$ convergence rate for the u solution error is satisfied and so the rate for the adjoint solution. In this case, the latter rate is even better than the expected one from (22). The SUPG scheme keeps the same convergence rate for both solutions, while the other schemes RD-LDA and BUBBLE show a order 2 for $p = 1$ and 1 for $p > 1$.
Let now examinate the convergence rates for functionals. We consider the general linear problem (1) and its numerical discretization (9), where the bilinear form $\mathcal{B}(\cdot,\cdot)$ is continuous on $\mathcal{V}$ with respect to a specific $|||\cdot|||$-norm, i.e.

$$\mathcal{B}(w, v) \leq C_B |||w||| \, |||v||| \quad \forall w, v \in \mathcal{V} \tag{20}$$

Because the discretization is consistent and thus, the Galerkin orthogonality is satisfied, we assume that following *a priori* error estimate in the $|||\cdot|||$-norm holds: there are constants $C > 0$ and $r = r(p) > 0$ such that, for $\forall u \in H^{p+1}(\Omega)$

$$|||u - u_h||| \leq Ch^r |u|_{H^{p+1}(\Omega)} \tag{21}$$

Finally, we assume that the projection operator $P^b_{h,p}$ satisfies following approximation estimate in the $|||\cdot|||$-norm: there are constants $C > 0$ such that, for $\forall v \in L^2(\Omega)$

$$|||v - P^b_{h,p}v||| \leq Ch\|v\|_{L^2(\Omega)} \tag{22}$$

Let then assume that the target quantity as described in (2) with j_Ω and $\jmath_\Gamma$ smooth functions on Ω and Γ, respectively. Then we have following estimate

$$\begin{aligned} |J(u) - J(u_h)| &= |\mathcal{B}(u - u_h, z)| \\ &= |\mathcal{B}(u - u_h, z - P^b_{h,p}z)| \\ &\leq Ch^{r+1}|u|_{H^{p+1}(\Omega)}\|v\|_{L^2(\Omega)} \end{aligned} \tag{23}$$

Once again, to numerically verify the convergence rate of functionals for a Petrov-Galerkin scheme let consider the circular advection problem [7] whose results are tabulated on tables 1 and 2.
The $p + 1$ order for the functional error is satisfied by RD and BUBBLE schemes, while for SUPG a superconvergence rate $2p + 1$ is obtained. This behaviour seems to be strictly connected to the higher order of the corresponding adjoint solution of this scheme.

4. Error Representation Formula

Let consider the primal numerical problem (9) and that holds the *Galerkin orthogonality condition* (14). Let then notice that by the *compatibility condition* (3), using infinite-dimentional trial and test space, the adjoint problem can be redefined as

$$\mathcal{B}(w, z) = J(w) \qquad \forall w \in \mathcal{V}$$

So, an exact error representation formula for a given functional $J(\cdot)$ results from the following steps, where P_h denotes any suitable projection operator (i.e. interpolation, L_2 projection) into $\mathcal{V}^b_{h,p}$,

$$\begin{aligned} J(u) - J(u_h) &= J(u - u_h) \\ &= \mathcal{B}^*(z, u - u_h) \\ &= \mathcal{B}(u - u_h, z) \\ &= \mathcal{B}(u - u_h, z - P_h z) \\ &= \mathcal{B}(u, z - P_h z) - \mathcal{B}(u_h, z - P_h z) \\ &= F(z - P_h z) - \mathcal{B}(u_h, z - P_h z) \end{aligned} \tag{24}$$

so in summary

$$J(u) - J(u_h) = F(z - P_h z) - \mathcal{B}(u_h, z - P_h z) \qquad (25)$$

where no dependence on the exact solution u appears. Comptutationally, this error representation formula is not suitable for obtaing computable *a posteriori* error estimation unless the function $z - P_h z$ is unknown, since $z \in \mathcal{V}^b$ is a solution of the infinite-dimensional adjoint problem. So z has to be computed by the discrete adjoint problem (10). Since (7) holds, we can solve the adjoint problem by using the same bilinear operator, $\mathcal{B}(w_h, z)$, used for the primal problem. Due to the Galerkin orthogonality, the adjoint numerical problem must be approximated in a larger space of functions than that utilized in the primal numerical problem. Here, this is achieved by solving the adjoint problem using a polynomial space that is one polynomial degree higher than the primal numerical problem, i.e. if $v_b \in \mathcal{V}^b_{h,q}$ then $z \approx z_{b'} \in \mathcal{V}^b_{h,q+1}$.
The error representation formula written in the global abstract form of the (25) does not indicate which elements in the mesh should be refined to reduce the measured error in a functional. So, now the goal is to estimate the *local* contribution of each element in the mesh to the functional error. This local cell contribution will then be used as an error indicator for choosing which elements to refine or coarsen in the adaptive mesh procedure. By applying the *triangle inequality*, indeed, we have

$$\left|J(u) - J(u_h)\right| \leq \sum_{\kappa \in \mathcal{K}} \left|F_\kappa(z - P_h z) - \mathcal{B}_\kappa(u_h, z - P_h z)\right| \qquad (26)$$

where

$$F_\kappa(z - P_h z) - \mathcal{B}_\kappa(u_h, z - P_h z) = \mathcal{R}_\kappa(u_h, z - P_h z)$$

and

$$\mathcal{R}_\kappa(u, v) = (R(u), v)_\kappa + (r(u), C^* v)_{\partial\kappa \cap \Gamma}$$

with $R(u) = f - Lu$ and $r(u) = g - Bu$. This direct estimate let define for each partition element κ the *adaptation element indicator* η_κ

$$|\eta_\kappa| \equiv \left|\mathcal{R}_\kappa(u_h, z - P_h z)\right| \qquad (27)$$

Adaptive Meshing. Now, we consider the design of an adaptive algorithm to compute efficiently a given target quantity functional $J(\cdot)$. The simplest adaptation stopping criterion will be

$$|J(u) - J(u_h)| \leq \mathsf{TOL}$$

with TOL a given tolerance. To this aim, we employ the approximate error bound $\sum_{\kappa \in \mathcal{K}} |\eta_\kappa|$ to estimate when the desired level of accuracy has been achieved. Then, we practically enforce

$$\sum_{\kappa \in \mathcal{K}} |\eta_\kappa| \leq \mathsf{TOL}$$

Hence, a simple mesh adaptation strategy can be outlined as follows:

1. Construct an initial mesh $\mathcal{K}$.
2. Compute the numerical approximation $u_h \in \mathcal{V}_{h,p}$ on the current mesh $\mathcal{K}$.
3. Compute the numerical approximation $z_b \in \mathcal{V}^b_{h,q}$ on the same current mesh $\mathcal{K}$ and where $q > p$.
4. Evaluate the error indicators, η_κ, for all elements $\kappa \in \mathcal{K}$ and sum them all up.
5. If $\sum_{\kappa \in \mathcal{K}} |\eta_\kappa| \leq \mathsf{TOL}$ where TOL is a given tolerance, then STOP.
6. Otherwise, refine and coarsen a specified fraction of the total number of elements according to the size of $|\eta_\kappa|$, generate a new mesh $\mathcal{K}$ and GOTO 2.

5. Numerical Results

In this section, selected numerical examples are given for scalar advection (and/or reaction) problems. SUPG, RD and bubble schemes are the numerical schemes used for all cases. The following tables tabulate values of the functional error and the estimated error as given in (26) using numerically approximated adjoint problems.
In addition, an effictivity index is included to characterize the sharpness of the current estimates

$$\theta_{\text{eff}} = \frac{|\text{estimated error}|}{|J(u) - J(u_h)|} \qquad (28)$$

When the exact adjoint solution is used

$$|J(u) - J(u_h)| = \Big|\sum_{\kappa \in \mathcal{K}} \eta_\kappa\Big|$$

so the corresponding column in the following tables measures the effect of numerically approximating the adjoint problem. After application of the triangle inequality, the estimate

$$|J(u) - J(u_h)| \leq \sum_{\kappa \in \mathcal{K}} |\eta_\kappa|$$

is obtained. Mesh adaptation strategies are usually based on $|\eta_\kappa|$ and so they depend on this error estimation. As internal cancellations are precluded, the estimate can usually lose in accuracy. Hence, column six and seven of the following tables show the current estimate and its efficiency index.

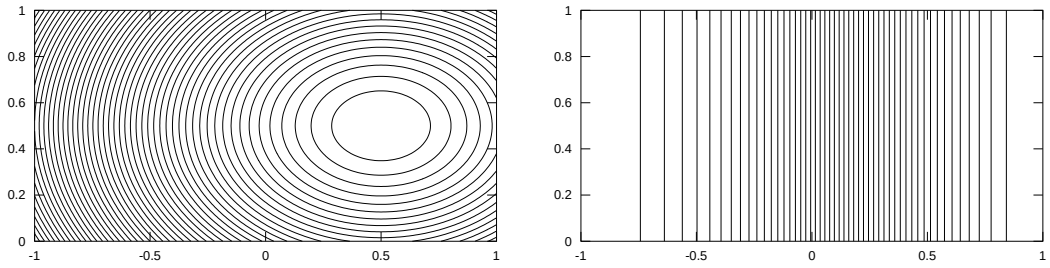

(a) (b)

Figure 2: Reaction problem : (a) primal; (b) adjoint

Method	h	$\lvert J(u) - J(u_h)\rvert$	$\lvert \sum_\kappa \eta_\kappa \rvert$	(θ_{eff})	$\sum_\kappa \lvert \eta_\kappa \rvert$	(θ_{eff})
SUPG	.0625	4.4835e-07	1.2320e-07	(0.27)	6.2854e-06	(14.0)
SUPG	.0312	4.8891e-08	1.2628e-08	(0.26)	1.4880e-06	(30.4)
SUPG	.0156	5.4553e-09	1.2829e-09	(0.24)	3.6255e-07	(66.5)
SUPG	.0078	6.3152e-10	1.3283e-10	(0.21)	8.9566e-08	(141)
RD-LDA	.0625	2.3770e-05	1.9639e-05	(0.83)	2.0265e-05	(0.85)
RD-LDA	.0312	5.9543e-06	4.9327e-06	(0.83)	5.0964e-06	(0.86)
RD-LDA	.0156	1.4910e-06	1.2368e-06	(0.83)	1.2757e-06	(0.86)
RD-LDA	.0078	3.7312e-07	3.0974e-07	(0.83)	3.1908e-07	(0.86)
BUBBLE	.0625	5.9175e-06	3.2404e-06	(0.55)	4.0190e-06	(0.68)
BUBBLE	.0312	1.4556e-06	7.9155e-07	(0.54)	9.7550e-07	(0.67)
BUBBLE	.0156	3.6096e-07	1.9585e-07	(0.54)	2.4039e-07	(0.67)
BUBBLE	.0078	8.9876e-08	4.8773e-08	(0.54)	5.9721e-08	(0.66)

Table 3: Efficiency rates $p_{\text{p}} = 1$ and $p_{\text{a}} = 2$ order of the SUPG, RD and BUBBLE methods error estimates for the advection reaction problem.

Method	h	$\lvert J(u) - J(u_h)\rvert$	$\lvert \sum_\kappa \eta_\kappa \rvert$	(θ_{eff})	$\sum_\kappa \lvert \eta_\kappa \rvert$	(θ_{eff})
SUPG	.0625	7.4432e-08	7.2144e-08	(0.97)	8.8806e-08	(1.19)
SUPG	.0312	1.0126e-08	9.8401e-09	(0.97)	1.1740e-08	(1.16)
SUPG	.0156	1.3178e-09	1.2815e-09	(0.97)	1.5062e-09	(1.14)
SUPG	.0078	1.6795e-10	1.6335e-10	(0.97)	1.9061e-10	(1.13)
RD-LDA	.0625	2.0983e-08	1.8213e-08	(0.87)	2.4471e-08	(1.17)
RD-LDA	.0312	2.6073e-09	2.2146e-09	(0.85)	3.0422e-09	(1.17)
RD-LDA	.0156	3.2153e-10	2.6966e-10	(0.84)	3.7474e-10	(1.17)
RD-LDA	.0078	3.9683e-11	3.3028e-11	(0.83)	4.5879e-11	(1.16)
BUBBLE	.0625	1.3311e-08	1.3106e-08	(0.98)	1.6135e-08	(1.21)
BUBBLE	.0312	1.5441e-09	1.4984e-09	(0.97)	1.9342e-09	(1.25)
BUBBLE	.0156	1.8277e-10	1.7538e-10	(0.96)	2.3381e-10	(1.28)
BUBBLE	.0078	2.1956e-11	2.0914e-11	(0.95)	2.9851e-11	(1.36)

Table 4: Efficiency rates $p_{\text{p}} = 2$ and $p_{\text{a}} = 3$ order of the SUPG, RD and BUBBLE methods error estimates for the advection reaction problem.

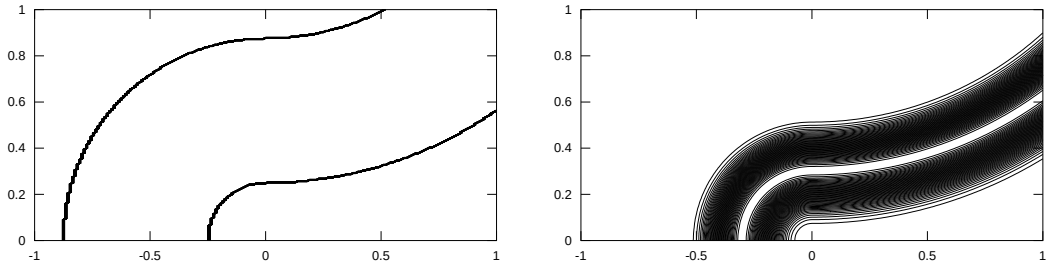

(a) (b)

Figure 3: Analytical solutions linear hyperbolic problem [4]: (a) primal; (b) adjoint

Advection-reaction. The advection-reaction case is defined by the following linear equation

$$\begin{aligned} \boldsymbol{b}\cdot\nabla u + cu &= f \quad \text{in } \Omega \\ u &= g \quad \text{on } \Gamma_- \end{aligned} \tag{29}$$

with $\boldsymbol{b} = (1, 0)$, $c = 1 - \text{sign}(x)x$. The source term f is given such that the analytical solution u^* of (29) is as follows

$$u^* = \alpha e^{-[a(x-x_0)^2 + b(y-y_0)^2]}$$

Finally, boundary conditions are consistent by the analytical solution. Once again the target quantity is an outflow functional such that the corresponding adjoint problem becomes

$$\begin{aligned} \boldsymbol{b}\cdot\nabla z + cz &= 0 \quad \text{in } \Omega \\ z &= 1 \quad \text{on } \Gamma_+ \end{aligned}$$

Figures 2a and 2b show primal and adjoint solutions, respectively, while error estimation data are tabulated on tables 3 and 4. Here, RD-LDA scheme seems to be the best scheme with all estimates which keep close to exact functional error. What sounds odd is the $p = 1$ SUPG estimate which seems out of control. This becomes even more weird by looking to the $p = 2$ estimate where both thetas converge to one.

Hartmann's problem. With the following example, we compare the efficiency of the adjoint based error estimation, in adaptive meshing, with respect to the *ad hoc* estimation procedure.
Let consider the linear hyperbolic problem ([4]):

$$\begin{aligned} \boldsymbol{b}\cdot\nabla u &= f \quad \text{in } \Omega \\ u &= g \quad \text{on } \Gamma_- \end{aligned} \tag{30}$$

with the advection $\boldsymbol{b} = \frac{\tilde{\boldsymbol{b}}}{|\tilde{\boldsymbol{b}}|}$, where

$$\tilde{\boldsymbol{b}} = \begin{cases} (y, -x), & \text{for } x < 1, \\ (2 - y, x) & \text{otherwise} \end{cases}$$

The analytical solution is shown in figure 3a, where the two discontinuites of the two inlet jumps are carried along the charactistic directions of the advection field. Let then suppose to be interested in the solution along the outlet boundary segment $1/4 \le y \le 1$. We solve numerically both problems by the SUPG scheme $p = 2$ and $p = 3$ order, respectively for primal and adjoint problem. Figure 4 shows the numerical solutions and the corresponding final adaptive meshes, generated by the *ad hoc* residual error indicators, $\eta_\kappa^{\text{ad hoc}}$, and the current adjoint weighted-ones, η_κ^{adj}, respectively. In figure 4c we see how the final mesh is refined along both discontinuites, giving a very good resolution for the both corresponding jumps, see figure 4a. Instead, the mesh coming out from the based adjoint error estimation refines only in the neighborhood of the lower jump, see figure 4d, the one which goes out through the target outlet. The other jump is then roughly solved but, as the adjoint solution over that zone is null, the error of the solution along the second jump do not affect the current target quantity. This is the reason why it is not refined during the adaptation.
Comparing the two procedures, the adjoint-based estimation proves to be more efficient, since it reaches a similar accuracy of the target quantity: $|J(e)| = 2.4697 \times 10^{-8}$ vs. $|J(e)| = 1.3100 \times 10^{-6}$, generating a final mesh with roughly half of the elements: 1771 instead of 3736. Moreover, figure 5 shows how the target quantity error of the adjoint refinement always remains inferior to the *ad hoc* one. However, we must remind to that this algorithm needs to solve two

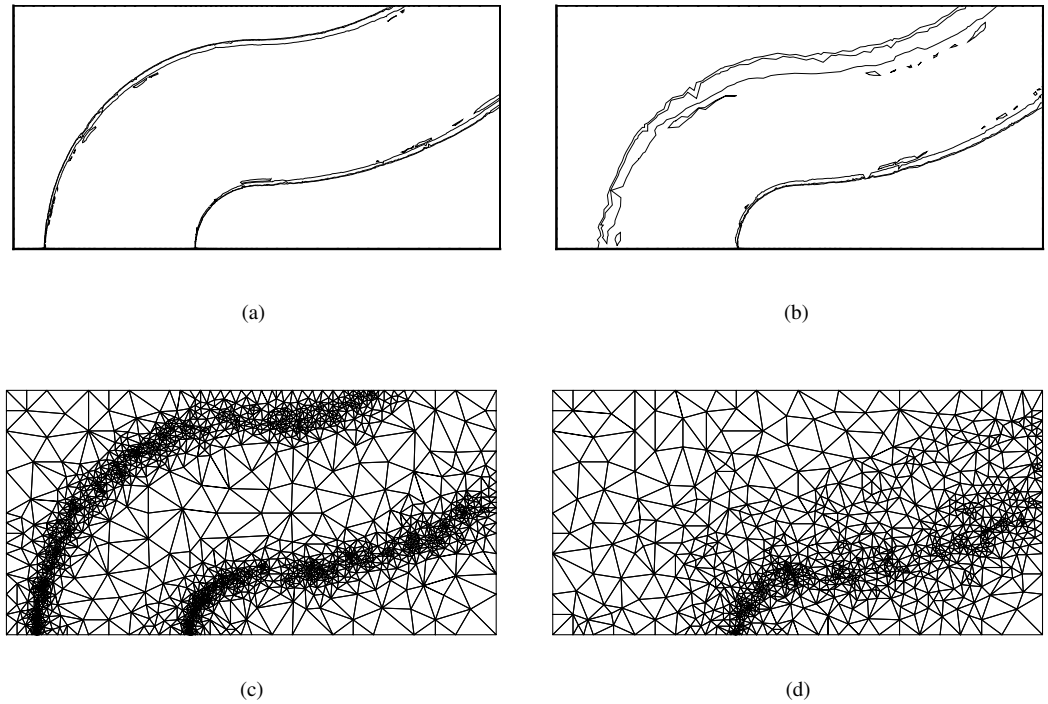

Figure 4: Adaptive refinement for the hyperbolic linear problem (30): (a) Numerical solution solved on the mesh (c), generated by a based-residual error estimation; (b) Numerical solution solved on the mesh (d), generated by the adjoint error estimation;

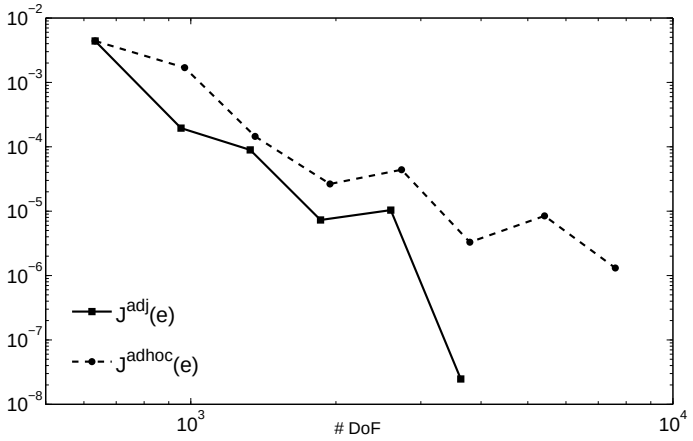

Figure 5: Convergence of the target quantity error, $J(e)$

problems, primal and adjoint, while the simple based-residual estimation solves the only primal one. Since, in this case, both problems are linear and the adjoint is solved with an higher order, the added computational cost can be remarkable. Anyway, this cost will become negligible for non-linear primal problem as the adjoint will be still linear.

6. Conclusions

Among different types of error representation formula, we were interested in Type I error indicator. Unlike Type II error bounds where the only local residual is taken into account, Type I involves also the solution of the associated adjoint problem. By it, we are able to obtain further information concerning the trasport of the error of computing the quantity of interest.
For the first time, we apply this to error analysis by using a Petrov-Galerkin discretization. Some schemes are then implemented: Streamline Upwind PG, Residual Distribution and a bubble scheme. Theory proves that the convergence rate of the target quantity error depends on the chosen scheme. Few linear problems have been employed to verify the behaviour of these schemes, while an hyperbolic problem has been used to test the efficiency of the current refinement with respect to the classical residual based estimation. Now, further extensions to non-linear hyperbolic problems are possible.

References

[1] P. H. K. Eriksson, D. Estep, C. Johnson, Introduction to adaptive methods for different equations, Acta Numerica (1995) 105–158.

[2] R. Becker, R. Rannacher, A feed-back approach to error control in finite element methods: basis analysis and examples, Journal Numerical Mathematics 4 (1996) 237–264.

[3] R. Becker, R. Rannacher, An optimal control approach to a-posteriori error estimation in finite element methods, Acta Numerica 10 (2001) 1–102.

[4] R. Hartmann, Adaptive finite element methods for the compressible euler equations, Ph.D. thesis, Universität Heidelberg (2002).

[5] R. Hartmann, Numerical analysis of higher order discountinuos galerkin finite element methods, in: 35th CFD VKI / ADIGMA, 2008.

[6] M. Giles, N. Pierce, Adjoint equations in cfd: duality, boundary conditions and solution behaviour, AIAA (1997) 97–1850.

[7] T. Barth, *A Posteriori* error estimation and mesh adaptivity for finite volume and finite element methods, Tech. rep., NASA Ames Research Center (2002).

High–order RDS and p-multigrid Solution Algorithms for Compressible Flow

Martin Vymazal

Aeronautics and Aerospace Department, von Karman Institute for Fluid Dynamics, Belgium, martin.vymazal@vki.ac.be

Supervisor: Herman Deconinck

Professor, Aeronautics and Aerospace Department, von Karman Institute for Fluid Dynamics, Belgium, deconinck@vki.ac.be

University Supervisor: Chris Lacor

Professor, Department of Mechanical Engineering, Faculty of Applied Sciences, Vrije Universiteit Brussel, Belgium, Chris.Lacor@vub.ac.be

Abstract

Residual distribution schemes are discussed in the context of higher order spatial discretization for hyperbolic conservation laws. The discrete solution is approximated by a finite element space based on triangular Lagrangian P_k elements. A natural subtriangulation of these elements allows the reuse of simple distribution formula previously developed for linear P_1 triangles. Curved elements with piecewise quadratic and cubic approximation of the boundaries of the domain are considered.

In the second part, a new variant of RD scheme is proposed. This particular formulation avoids the sub–triangulation procedure.

Keywords: residual distribution, multidimensional upwind, high order, curvilinear geometry

1. Introduction

The present work follows a Residual Distribution approach (1; 2; 3), which is close to continuous finite element methods, but allows the use of a maximum principle to construct nonlinear monotonicity preserving and truely multidimensional stabilizations. In previous papers (4) we have exploited the close relation with continuous finite element discretizations to present a class of higher order residual distribution methods defined on P_k Lagrangian triangular finite elements. Here we focus on the use of curved elements to allow for a higher order representation of the boundaries of the domain, using sub- or isoparametric transformation from physical space to a Cartesian parent element.

2. Notations

We consider the steady state solution of a conservation law on a two–dimensional spatial domain Ω:

$$\frac{\partial \boldsymbol{u}}{\partial t} + \nabla \cdot \boldsymbol{\mathcal{F}} = 0 \quad \forall (x, y) \in \Omega \subset \mathbb{R}^2, \quad \forall t \geq 0, \quad (1)$$

where $\boldsymbol{u}$ is the vector of conserved variables and $\boldsymbol{\mathcal{F}}$ is the inviscid flux vector, $\boldsymbol{\mathcal{F}}(\boldsymbol{u}) = (\mathbf{f}(\boldsymbol{u}), \mathbf{g}(\boldsymbol{u}))$. We denote by $\mathcal{T}_{h,k}$ a triangulation of the domain Ω, whereby each triangular element T of the triangulation $\mathcal{T}_{h,k}$ is a Lagrangian P_k finite element equipped with $K = \frac{(k+1)(k+2)}{2}$ degrees of freedom.

In the simplest case the geometry of the P_k triangle is considered to be linear, defined by its three corner nodes. Hence, the intermediate nodes on the boundary of the element are all located on the straight edges and therefore the boundary of the domain Ω is approximated by a polygone. Such a discretization will be denoted as a P_1P_k discretization (P_1 for geometry and P_k for the solution).

We work with elements whose edges are described by second- and third- order polynomials. Elements with quadratic geometry will be denoted as P_2P_k elements (P_2 for geometry and P_k for the solution). P_2P_2 elements are called isoparametric, while P_2P_k with $k > 2$ are called subparametric elements. The notation for P_3 elements is analogous.

The geometry of the curvilinear P_2 (P_3) element is transformed to a parent element in ξ–η space. In our

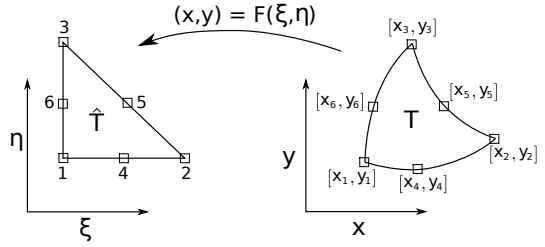

Figure 1: Transformation of triangle geometry from physical to reference space using Lagrange shape functions

case, we define $\mathbf{F}(\xi, \eta)$ from figure (1) as isoparametric mapping

$$\begin{bmatrix} x(\xi,\eta) \\ y(\xi,\eta) \end{bmatrix} = \sum_{i=1}^{N} \varphi_i^{h,k}(\xi,\eta) \cdot \begin{bmatrix} x_i \\ y_i \end{bmatrix} \tag{2}$$

where N is the number of degrees of freedom of P_2 or P_3 triangle, respectively. The number k refers to the order of shape functions φ_i and x_i, y_i denote the nodal coordinates of the triangle.

3. Residual Distribution method

For any triangulation $\mathcal{T}^{h,k}$ the cell residual for a given triangle is defined as the integral over the triangle of the spatial operator:

$$\begin{aligned} \phi^T &= \int_T \nabla \mathcal{F}(u^{h,k})\, d\Omega = \oint_{\partial T} \mathcal{F}(u^{h,k}) \cdot \vec{n}\, dl \\ &= \sum_{s=0}^{N_s} \int_{T_s} \vec{a}(u^{h,k}) \cdot \nabla u^{h,k}\, dx\, dy \\ &\qquad (N_s \ldots \text{number of sub–elements}) \end{aligned} \tag{3}$$

where we have used the expression for the Jacobian of the flux $\mathcal{F}(u)$ in (1),

$$\vec{a}(u) = \frac{\partial \mathcal{F}(u)}{\partial u} = \left(\frac{\partial f_1(u)}{\partial u}, \frac{\partial f_2(u)}{\partial u} \right) \tag{4}$$

We can also construct the residual over each P_1 sub-element of $\mathcal{T}^{h,k}$

$$\phi^{T_s} = \oint_{\partial T_s} \mathcal{F}(u^{h,k}) \cdot \vec{n}\, dl \tag{5a}$$

$$= \int_{T_s} \vec{a}(u^{h,k}) \cdot \nabla u^{h,k}\, dx\, dy \equiv \vec{a}^* \cdot \int_{T_s} \nabla u^{h,k}\, dx\, dy \tag{5b}$$

with $\vec{a}^*$ a properly defined local average of $\vec{a}(u)$ over the sub-triangle such that conservation is preserved (5). The existence of such local average for general nonlinear conservation law is not guaranteed, but in case of the conservation law (1) applied to the Euler equations considered in this work, a conservative linearisation is possible under the assumption that the vector of Roe variables changes linearly in each cell.

The basic idea of the residual distribution (RD) method consists of distributing fractions of this cell residual to the three nodes of the element T. The fraction sent to node $i \in T$ is denoted ϕ_i and we require

$$\sum_{i \in T} \phi_i = \phi^T \tag{6}$$

This requirement can be written in terms of *distribution coefficients* β_i which for consistency sum to unity

$$\sum_{i \in T} \beta_i = 1, \qquad \beta_i = \frac{\phi_i}{\phi^T} \tag{7}$$

After assembling all contributions in the nodes, the nodal equation for node i reads, with $\mathcal{D}_i$ the set of all triangles that share node i:

$$\sum_{T \in \mathcal{D}_i} \phi_i = 0 \tag{8}$$

Since the distribution is restricted to the nodes of the triangle itself, the stencil of the scheme remains compact. This equation can be solved by embedding in a pseudo–time iteration, i.e. by finding a steady state solution of

$$|S_i| \frac{du_i}{d\tau} + \sum_{T \in \mathcal{D}_i} \phi_i^T = 0, \tag{9}$$

where $|S_i|$ is the area of median dual cell.

3.1. Residual Distribution schemes on P_1 elements

For a given P_1 (both solution and geometry) triangle we consider the set of normal vectors $\{\vec{n}_j\}_{j \in T}$, defined by the inward normals to the edges of T facing each node $j \in T$ (see figure 2 left). The norm of $\vec{n}_i$ is equal to the length of the edge. Let us define the upwind parameter

$$k_j = \frac{1}{2} \vec{a}^* \cdot \vec{n}_j \quad \text{implying} \quad \sum_{i \in T_s} k_i = 0 \tag{10}$$

In this case, using a conservative linearisation (eq. 5b, 10), we can express the cell residual as follows:

$$\phi^T = \oint_{\partial T} \mathcal{F}(u^{h,1}) \cdot \vec{n}\, dl = \int_T \nabla \mathcal{F}(u^{h,1})\, d\Omega = \sum_{i \in T} k_i u_i \tag{11}$$

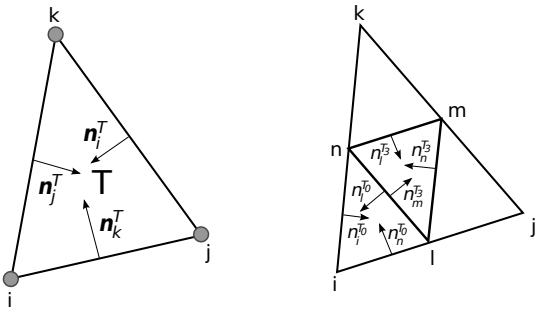

Figure 2: Definition of the normal vectors $\vec{n}_i$ in P_1 and P_2 elements

When all contributions for a given node are assembled, we end up with the following system of nodal equations, similar to equation (9), to be solved using explicit or implicit pseudo-time iterations. For example, using forward Euler method, we get:

$$|S_i|\frac{u_i^{n+1}-u_i^n}{\Delta\tau}+\sum_{T_s,\ i\in T_s}\phi_{i,n}^{T_s}=0 \tag{12}$$

Many distribution schemes (defining the split residuals ϕ_i) for P_1 elements have been developed in the past (4; 6; 7). A particular class satisfies a multidimensional upwinding property (MU). Such distributions satisfy the requirement that a node in a triangle does not receive a contribution if its opposed face is an outflow face. The condition is easily imposed by requiring $\phi_i = 0$ whenever $k_i < 0$. Within this work, we limited ourselves to the use of the LDA (Low Diffusion A) scheme. Denoting by k_i^+ and k_i^- the positive and negative part of the upwind parameter, $k^\pm = \frac{k\pm|k|}{2}$, the distribution coefficients of the LDA scheme can be written as

$$\beta_i^{LDA}=\frac{k_i^+}{\sum_{m=1}^3 k_m^+} \tag{13}$$

This scheme is of order $O(k+1)$ (k being the order of interpolating polynomial), but not strictly monotone. We refer the reader interested in detailed description of the LDA scheme to other literature (1; 8; 4; 6; 9).

3.2. Residual distribution schemes on P_1P_k elements

Consider now the extension of multidimensional upwind (MU) schemes to high order P_1P_k elements. We will assume that the inward normals $\vec{n}_j$'s are defined on the local P_1 sub-elements $T_s \in T$, as shown on figure 2 (right) for $k = 2$. Note that if we consider a P_1P_k element (P_k element for the solution but only P_1 triangles for the geometry, defined by the 3 corner nodes), the inward normals of the sub-elements can be deduced easily from the ones of the parent element by a simple rescaling. We compute the residual on each sub-element:

$$\phi^{T_s}=\int_{T_s}\nabla\mathcal{F}(u^{h,k})\,d\Omega=\oint_{\partial T_s}\mathcal{F}(u^{h,k})\cdot\hat{n}\,dl \tag{14}$$

Then, this residual is distributed to the 3 nodes of the sub-element, using the LDA distribution scheme (13) developed for P_1 triangles:

$$\phi_i^{T_s,LDA}=\beta_i\phi^{T_s} \tag{15}$$

The linearization used to compute the parameters k_i can be based on any linearized state over the sub-triangle, without affecting accuracy nor conservation.

Remark. *This is not the only strategy to achieve residual distribution schemes on P_k elements. In particular, we refer to Lax Friedrichs distribution schemes of Abgrall and collaborators (10), (11). In this case the residual is computed on the complete P_k element and then distributed to the N nodes of the element without making use of a sub-triangulation.*

3.3. Curvilinear P_2P_k and P_3P_k elements

We consider elements where the geometry is either piecewise quadratic or cubic. The geometry and numerical solution can be discretized independently so in general the solution can have any order k. However, we focus on isoparametric (P_2P_2 or P_3P_3) high–order elements.

To ensure conservation of fluxes, we compute the sub-element residual from equation (14) as a contour integral:

$$\phi^{T_s}=\oint_{\partial T_s}\mathcal{F}(u^{h,k})\cdot\vec{n}\,dl \tag{16}$$

The boundary ∂T_s is described by transformation (2). For every face on ∂T_s, this transformation is a function of only one parameter ζ:

$$\begin{aligned}x&=x(\zeta)\\ y&=y(\zeta)\end{aligned} \tag{17}$$

We integrate numerical the fluxes of (16) using Gauss quadrature: 3 points per face f of the sub–element for P_2 and 5 points for P_3:

$$\oint_f\mathcal{F}(u^{h,k})\cdot\vec{n}\,dl\simeq\sum_{q=1}^{N}w_q[\mathcal{F}(u_q)\cdot\vec{n}_q]J_q, \tag{18}$$

$$J_q=\sqrt{\dot{x}^2(\zeta_q)+\dot{y}^2(\zeta_q)} \tag{19}$$

where J_q is the Jacobian of transformation (17) at quadrature point q. We use the transformation also to compute the normal $\vec{n}_q$.

The integral over f in equation (18) is approximated:

- by three-point Gauss quadrature for each face of P_1P_1 triangle
- by the same quadrature for each face of each *sub–triangle* in the case of P_1P_2 and P_2P_2 elements
- by five–point Gauss quadrature on each sub–face of the P_3P_3 element

The quadrature nodes and weights on the biunit interval are given in table 1.

	Quadrature points	*Weights*
P_1P_1, $P_{1(2)}P_2$	0.0	$\frac{8}{9}$
	$\pm\sqrt{\frac{3}{5}}$	$\frac{5}{9}$
P_3P_3	0.0	0.5688888889
	±0.5384693101	0.4786286705
	±0.9061798459	0.2369268850

Table 1: Gauss quadrature used to approximate the residuals $\phi^{T,in}$.

3.4. Subsonic flow around a cylinder

We present results for a test case with stagnation point, namely the flow around a circular cylinder at $M_\infty = 0.38$. We consider four O–meshes with 16×5 (M1), 32×9 (M2), 64×17 (M3) and 128×33 (M4) points as described in (12). The first number indicates the number of nodes in the circular direction of the mesh, the second number refers to the number of nodes in the radial direction (figure 3). The radii of the circles in each mesh follow a geometric series

$$r_j = r_0\left(1 + \frac{2\pi}{128}\sum_{k=0}^{j-1}\alpha^k\right),\ j = 1, 2, \ldots 32, \qquad (20)$$

where $\alpha = 1.1648336$ and $r_0 = 0.5$ is the radius of the cylinder. The farfield boundary is located at 20 diameters from the center. To have the same number of degrees of freedom and make a fair comparison between the P_1P_1 and P_2P_2 schemes, we create a P_1 sub-triangulation of each P_2 triangle. The P_3P_3 meshes were created independently such that the number of *elements* is equal for P_1P_2, P_2P_2 and P_3P_3 meshes. We plot the P_1 solutions on all four meshes

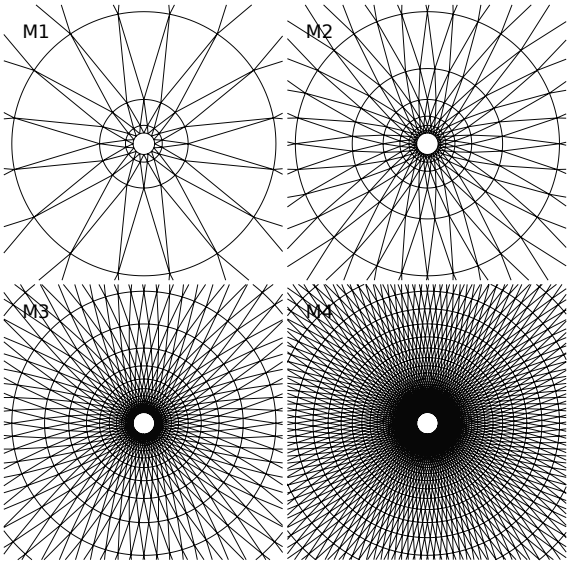

Figure 3: 16×5, 32×9, 64×17 and 128×33 meshes for subsonic cylinder test case.

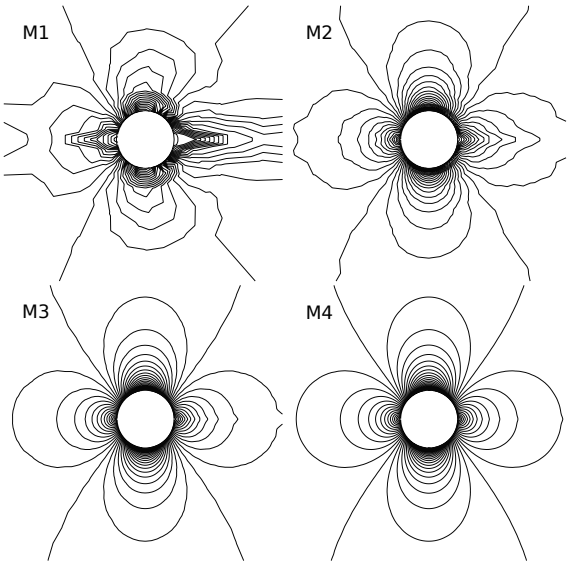

Figure 4: Mach isolines plotted for Ma $\in \langle 0, 1\rangle$, $\Delta Ma = 0.025$ on mesh with P_1P_1 elements.

(figure 4). Higher–order solution is shown in figure 5 for M2 and M3. Figure 6 presents the pressure coefficient on the cylinder wall and the entropy deviation on mesh M1. We measure the rate of convergence again by computing the relative decrease of the L_2 norm of entropy error Σ as the mesh is refined. The measured order is reported in figure 7. We did not include the entropy error on M1 in the computation of the convergence order of P_1P_2 discretization, since

this error is very large (all values are listed table 2). As a result, the convergence rate measured on all four meshes seems to be very high due to rapid decrease of the entropy error as the element size becomes small compared to the curvature of the cylinder.

		P_1P_1	P_1P_2
Mesh	NDOF	$\|\|\Sigma\|\|_{L_2}$	$\|\|\Sigma\|\|_{L_2}$
M1	288	4.87E -02	6.03E-02
M2	1088	7.64E -03	1.78E-03
M3	4224	1.13E -03	1.57E-04
M4	16640	1.78E -04	2.04E-05
Order		*1.99*	*3.05*

		P_2P_2	P_3P_3
Mesh	NDOF	$\|\|\Sigma\|\|_{L_2}$	$\|\|\Sigma\|\|_{L_2}$
M1	624	1.00E-02	1.46E-03
M2	2400	1.78E-03	5.62E-05
M3	9408	1.27E-04	5.35E-06
M4	37248	2.76E-05	5.33E-07
Order		*2.98*	*3.84*

Table 2: L_2 norm of entropy error (Σ): subsonic cylinder test case.

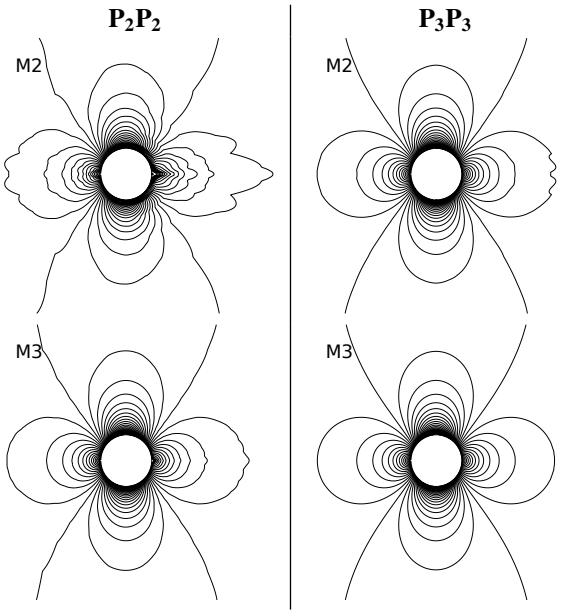

Figure 5: Mach number isolines plotted for $Ma \in \langle 0, 1 \rangle$, $\Delta Ma = 0.025$ on meshes M_2 and M_3. Left: P_2 elements, right: P_3 elements.

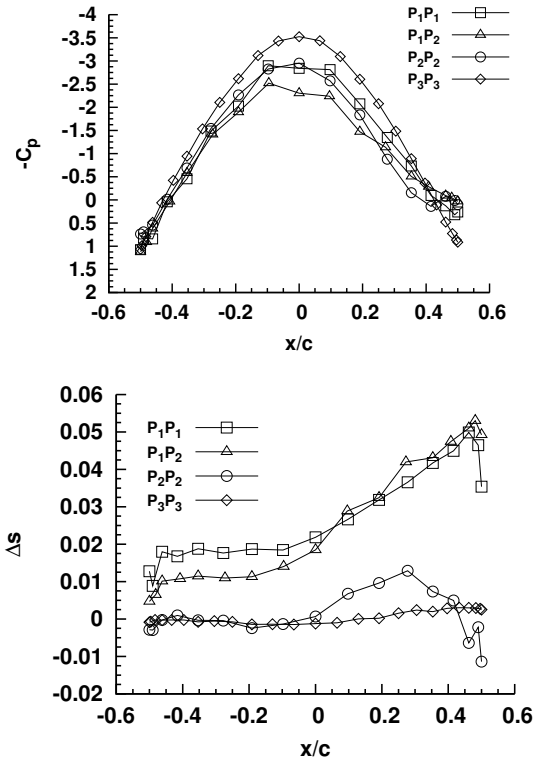

Figure 6: Pressure coefficient (left) and entropy deviation $s - s_{in}$ (right) on the cylinder wall on mesh M1

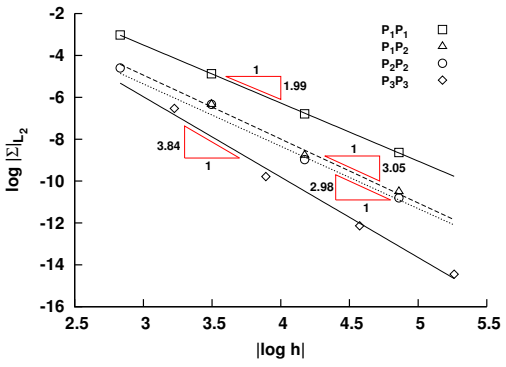

Figure 7: Subsonic cylinder test case; L_2 norm of the entropy error as a function of the mesh size h.

4. Residual distribution schemes with variable distribution coefficient

We consider a linear differential problem

$$\mathcal{L}u = f,$$

with for example $\mathcal{L} = \boldsymbol{\lambda}\cdot\nabla$ or $\mathcal{L} = \boldsymbol{\lambda}\cdot\nabla - \nu\Delta$. The numerical solution $u^{h,k}$, is a FE representation polynomial of the discrete solution:

$$u_h = \sum_{T\in\text{mesh}}\sum_{j\in T}\varphi_j u_j^{h,k}$$

When $k = 1$ ($u^{h,k}$ is a linear polynomial), RDS proceeds as follows

1. *Compute residual:*

$$\begin{aligned}\Phi^T &= \int_T \mathcal{L}u^h dX = \sum_{j\in T}\left(\int_T \mathcal{L}\varphi_j\, dX\right)u_j \qquad (21)\\ &= \sum_{j\in T} u_j \int_T k_j\, dX\end{aligned}$$

   defining k_j as

$$k_j = \mathcal{L}\varphi_j$$

2. *Distribution:* achieved eventually via the definition of coefficients $\beta_i^T = \beta_i^T(\{k_j\}_{j\in T}, u_h, \boldsymbol{\lambda}, h, \Phi^T)$
3. *Assembly/resolution:* obtain the values $\{u_j\}_{j\in\text{mesh}}$ as a solution of $\sum_{T|j\in T}\beta_j^T\Phi^T = 0$

In the linear case the derivatives of the basis functions are constants. This allows the following reinterpretation of the above scheme as a Petrov–Galerkin scheme with particular test functions.

1. Definition of the test function β:

$$k_j = \mathcal{L}\varphi_j, \quad \beta_j(x) = \beta_j^T(\{k_j\}_{j\in T}, u_h, \boldsymbol{\lambda}, h, r^T)$$
$$\text{with } r^T = \mathcal{L}u_h|_T$$

2. Integrate: $\Phi_i^T = \int_T \beta_i(x) r^T$
3. Assembly/resolution: get the values $\{u_j\}_{j\in\text{mesh}}$ by solving $0 = \sum_{T|j\in T}\Phi_i^T = \sum_{T|j\in T}\int_T \beta_i(x) r^K$

Since all the known definitions of β_i^T depend on the definition of k_j (i.e. on the derivatives of the shape functions), the two schemes are identical in the P^1 case. The schemes are not the same anymore for P^k interpolation, $k > 1$.

4.1. Conservation issues

In case we need apply the method to nonlinear conservation law

$$\nabla\cdot\boldsymbol{\mathcal{F}} = 0$$

a necessary condition for the scheme to converge to some weak solution is that

$$\sum_{j\in K}\varphi_j = \oint_{\partial K}\boldsymbol{\mathcal{F}}(u^{h,k})\cdot\boldsymbol{n}$$

is satisfied for some approximation of the *physical* flux $\boldsymbol{\mathcal{F}}$ which is continuous across element edges. One possible approach to satisfy this requirement is a suitable volume integration.

Suppose that the flux is approximated by Finite Element shape functions φ^F:

$$\boldsymbol{\mathcal{F}}(u^{h,k}) = \sum_{j\in K}\boldsymbol{\mathcal{F}}_j(u^{h,k})\varphi_j^F \qquad (22)$$

The Finite Element space which interpolates the discrete flux need not be the same as the Finite Element space used for the solution variable. However, it should be richer to account for the nonlinearity of the flux $\boldsymbol{\mathcal{F}} = \boldsymbol{\mathcal{F}}(u)$. Assuming the continuity of the flux function, the following relation is satisfied for exact integration

$$\int_K \nabla\cdot\boldsymbol{\mathcal{F}}(u^{h,k}) = \oint_K \boldsymbol{\mathcal{F}}(u^{h,k})\cdot\boldsymbol{n}$$

Since the flux is interpolated as described in equation (22), the following identity holds

$$\begin{aligned}\int_K \nabla\cdot\boldsymbol{\mathcal{F}}(u^{h,k}) &= \sum_{j\in K}\boldsymbol{\mathcal{F}}_j(u^{h,k})\cdot\int_K\nabla\varphi_j^F\\ &= \sum_{j\in K}\boldsymbol{\mathcal{F}}_j(u^{h,k})\cdot\sum_{q\in K}|K|w_q\nabla\varphi_j^F(x_q)\end{aligned}$$

The quadrature points x_q and weights w_q are chosen such that the gradients of flux shape functions are integrated exactly. The nodal residual is then evaluated as

$$\int_K \beta_i(x)\nabla\cdot\boldsymbol{\mathcal{F}}(u^{h,k}) = \sum_{j\in K}\sum_{q\in K}|K|w_q\beta_i(x_q)\boldsymbol{\mathcal{F}}_j(u^{h,k})\cdot\nabla\varphi_j^F(x_q)$$

4.2. Advantages of RD formulation with variable β

The RD schemes with variable distribution coefficient β work without any substantial modification not only on simplex elements, but also on tensor-product

elements (quadrilaterals in 2D). The construction of sub–elements used previously for the RD method becomes an important issue as the polynomial order of the underlying FE interpolation space becomes high (number of quadrature points per element quickly increases) and as we go to three dimensions (division into sub–elements becomes rather complex to implement in computer codes).

The generic formulation (21) avoids these problems and at the same time, it preserves the upwind nature of the original formulation of the RD schemes.

4.3. Examples of schemes

LDA

For the LDA scheme, we set

$$k_i = L\varphi_i = \boldsymbol{\lambda} \cdot \nabla \varphi_i, \qquad \beta_i^T = \frac{k_i^+}{\sum\limits_{j \in T} k_j^+}$$

and the nodal residual becomes

$$\Phi_i^T = \int\limits_T \frac{(L\varphi_i)^+}{\sum\limits_{j \in T} (L\varphi_j)^+} Lu_h \, dX$$

SUPG

Using the notation above, the SUPG residual can be written as

$$\Phi_i^T = \int\limits_T (\varphi_i + \tau L\varphi_i) Lu_h \, dX$$

with the upwind stabilization parameter $\tau = (\sum\limits_{i \in T} k_i^+)^{-1}$.

5. Scalar advection test case

Given a rectangular domain, we consider a steady advection equation

$$\lambda \cdot \nabla u = 0 \text{ with } \boldsymbol{\lambda} = (y, -x)$$

A cosinus profile is imposed at the inlet. The advection field is supposed to rotate this profile in the direction indicated in figure 8. The solution obtained with the LDA and SUPG schemes on a mesh consisting of P_2 triangles is depicted in figure 9.

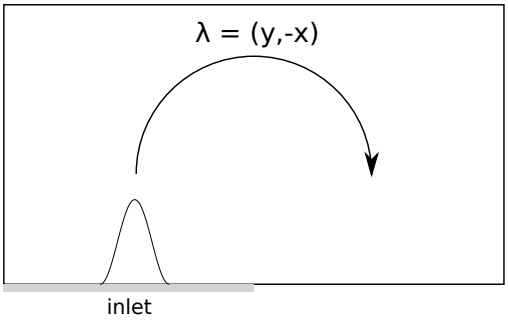

Figure 8: Setup for linear advection test case

6. Euler 2D test case

The extension of the scheme to a (nonlinear) system of equations was tested on a simple test case for Euler equations in 2D dimensions. Two supersonic states $\mathbf{u}_{L/R} = (\rho, \rho u, \rho v, E)_{L,R}$ are prescribed at the left and right half of the inlet (inlet boundary condition), and also in the left and right half of the whole domain as initial conditions (see figure 10). This test case was chosen because it does not require wall boundary condition, which are not implemented at this moment. The solution eventually forms an expansion fan (figure 11).

Acknowledgments

The presented results were obtained in collaboration with Tiago Quintino, Mario Ricchiuto and Nadège Villedieu. The construction of residual distribution schemes with variable β-coefficients as described in section 4 is due to an original idea of Mario Ricchiuto. No papers on this topic have been published so far.

References

[1] H. Deconinck, R. Abgrall, Introduction to residual distribution methods, VKI Lecture Series, Comput. Fluid Dynam., 2005.

[2] M. Ricchiuto, N. Villedieu, R. Abgrall, H. Deconinck, On uniformly high–order accurate residual distribution schemes for advection-diffusion, J. Comput. Appl. Math. 215 (2008) 547–556.

[3] H. Deconinck, K. Sermeus, R. Abgrall, Status of multidimensional upwind residual distribution schemes and applications in aeronautics, AIAA paper 2000-2328, AIAA CFD Conference, Denver (USA), June 2000.

[4] M. Ricchiuto, N. Villedieu, R. Abgrall, H. Deconinck, High–order residual distribution schemes: discontinuity capturing crosswind and extension to advection–diffusion, VKI Lecture Series, Comput. Fluid Dynam., 2005.

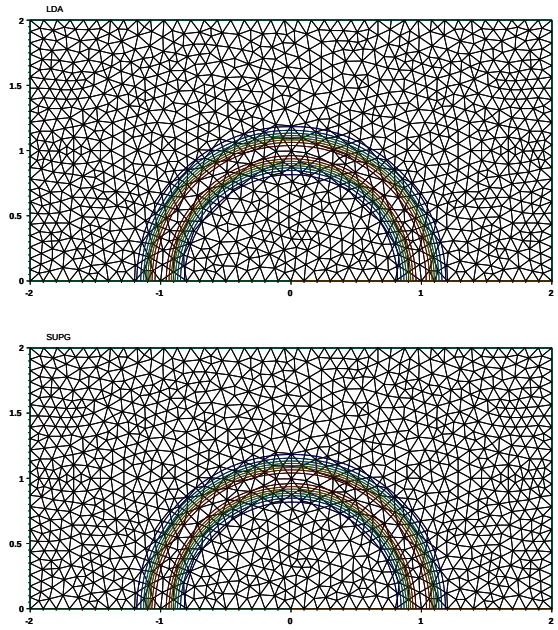

Figure 9: Linear advection test case - isolines of solution obtained with the LDA (top) and SUPG (bottom) schemes

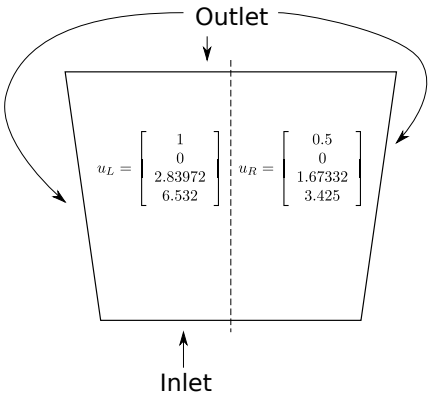

Figure 10: Initial and boundary conditions for the Euler 2D test case

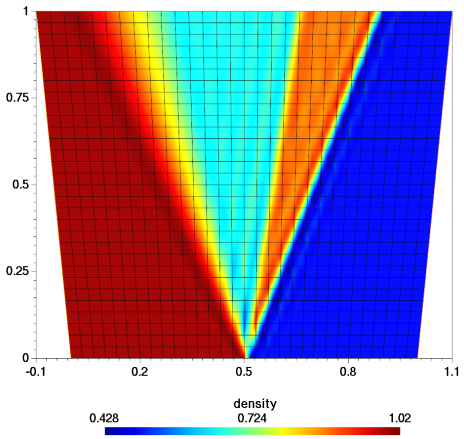

Figure 11: Solution of the Euler test case with LDA scheme on Q_2 elements

[5] H. Deconinck, P. L. Roe, R. Struijs, A multidimensional generalization of Roe's difference splitter for the Euler equations, Computers and Fluids 22(2/3) (1993) 215–222.

[6] H. Paillere, Multidimensional upwind residual distribution schemes for the Euler and Navier–Stokes equations on unstructured grids, Ph.D. thesis, Von Karman Institute for Fluid Dynamics and Université Libre de Bruxelles, Faculté des Sciences Appliquées (1995).

[7] E. van der Weide, H. Deconinck, Positive matrix distribution schemes for hyperbolic systems, with application to the Euler equations, Computational Fluid Dynamics (1996) 747–753.

[8] E. van der Weide, Compressible flow simulation on unstructured grids using multi–dimensional upwind schemes, Ph.D. thesis, Von Karman Institute for Fluid Dynamics and TU Delft (1998).

[9] N. Villedieu, T. Quintino, M. Vymazal, H. Deconinck, High-order residual distribution schemes: Unsteady and viscous terms, 35th Computational Fluid Dynamics Lecture Series, VKI/ADIGMA Course on High order Discretization Methods, Von Karman Institute for Fluid Dynamics, 2008.

[10] R. Abgrall, A. Lerat, M. Ricchiuto, C. Tavé, A simple construction of very high order non-oscillatory compact schemes on unstructured meshes, Computers and Fluids 38(7) (2009) 1314–1323.

[11] R. Abgrall, Residual distribution schemes: Current status and future trends, Computers and Fluids 35(7) (2006) 641–669.

[12] F. Bassi, S. Rebay, High–order accurate discontinuous finite element solution of the 2D Euler equations, J. Comput. Phys. 138 (1997) 251–285.